



Manganese silicate based redox catalysts for greener ethylene production via chemical looping – oxidative dehydrogenation of ethane



Seif Yusuf, Luke Neal, Vasudev Haribal, Madison Baldwin, H. Henry Lamb, Fanxing Li*

Department of Chemical and Biomolecular Engineering, North Carolina State University, 911 Partners Way, Raleigh, NC, 27695-7905, United States

ARTICLE INFO

Keywords:

Oxidative dehydrogenation
Chemical looping
Ethane
Ethylene
Redox catalyst

ABSTRACT

The current study investigates manganese silicate based redox catalysts for ethane to ethylene conversion in a chemical looping oxidative dehydrogenation (CL-ODH) process. Facilitated by a two-step cyclic redox scheme, CL-ODH has the potential to overcome the drawbacks of traditional steam cracking including high energy consumption, coke formation, and significant CO₂ and NO_x emissions. In CL-ODH, lattice oxygen in manganese silicate based redox catalysts is used to combust the hydrogen formed from ethane dehydrogenation, enhancing ethylene formation and suppressing coke formation. The oxygen-deprived redox catalyst is subsequently regenerated with air, releasing heat to balance the overall heat requirement. The key to this process is an efficient redox catalyst with high selectivity and facile oxygen transport. In this study, redox catalysts with combined manganese and silica phases were tested. We report that redox catalysts with high manganese content are more effective for CL-ODH due to their higher oxygen capacity at reaction temperatures. Sodium tungstate was used as a promoter due to its effectiveness to suppress CO_x formation. Among the redox catalysts investigated, sodium tungstate promoted (1.7 wt.% Na) manganese silicate (Mn:Si molar ratio = 70:30) was the most effective, showing an ethylene selectivity of 82.6% and yield of 63.3%. Temperature programmed reaction (TPR) experiments indicate that the sodium tungstate promoter inhibits ethane activation on the surface of the redox catalyst and is selective towards hydrogen combustion. XPS analysis indicates that the manganese silicate redox catalysts have a smaller amount of near surface Mn⁴⁺ than previously studied manganese containing redox catalysts, leading to higher ethylene selectivity on the un-promoted redox catalysts. XPS also indicates that the reduction of the un-promoted redox catalysts leads to the consumption of silica and formation of inosilicate species. ASPEN Plus® simulations of the CL-ODH scheme using manganese silicate based redox catalysts indicate significant energy and emissions savings compared to traditional steam cracking: the overall energy consumption for ethylene production can potentially be reduced by 89% using the manganese silicate based redox catalyst in the CL-ODH process. Resulting from the significant energy savings, CO₂/NO_x emissions can be reduced by nearly one order of magnitude when compared to traditional steam cracking.

1. Introduction

Ethylene is an important commodity chemical with an annual production projected to increase from 150 million tons/year (in 2013) to 376 million tons/year by 2050 [1]. Ethylene is primarily used to manufacture various chemical products and intermediates such as polyethylene, vinyl chloride, ethylene oxide, and ethyl benzene [2]. Ethylene is almost exclusively produced through steam cracking, a commercial process where hydrocarbon feedstocks (ethane, propane, naphtha, or gas oil) undergo high temperature pyrolysis in the presence of diluting steam [3]. Ethane steam cracking is becoming a more attractive approach for ethylene production with the increasing availability of shale gas in the U.S., since ethane is the second most abundant

component in natural gas [4].

In ethane steam cracking, a mixed stream of ethane and steam is preheated and then fed into high temperature reactor tubes for gas-phase cracking reactions [5]. Despite the widespread use of this process in industrial applications, there are a number of challenges it faces. First, the single pass conversion of ethane is limited due to thermodynamic equilibrium and coke formation. The latter requires periodic shutdown of steam crackers for coke removal and maintenance [6]. Second, the cracking process is energy and pollutant intensive. Approximately 16 GJ of energy is required to produce each ton of ethylene due to the highly endothermic cracking reactions and the complexity in downstream separation of ethylene, hydrogen, hydrocarbon byproducts and unreacted ethane [2]. This energy demand is met through the

* Corresponding author.

E-mail address: fli5@ncsu.edu (F. Li).

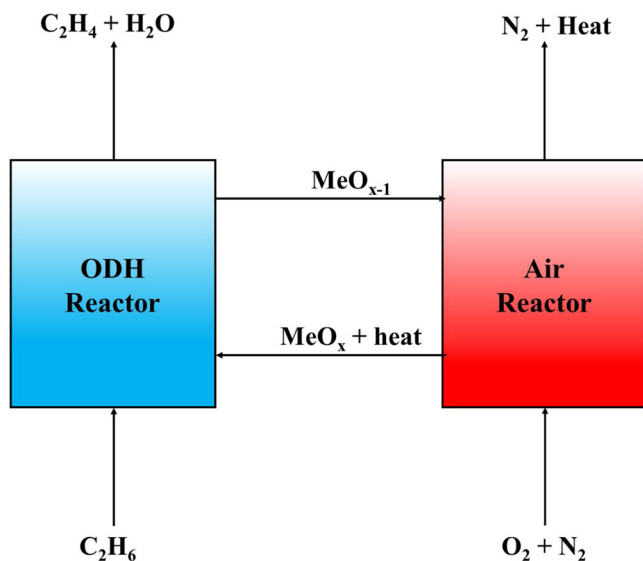


Fig. 1. Simplified Schematic of CL-ODH.

combustion of methane, leading to the emission of 1–1.2 ton CO_2 /tonne ethylene and significant amounts of NO_x [3].

The oxidative dehydrogenation (ODH) of ethane is an alternative to steam cracking for ethylene production [5,7–10]. In ethane ODH (Reaction 1), gaseous oxygen is used to combust hydrogen to remove equilibrium constraints on ethane conversion and make the overall reaction exothermic ($\Delta H^{850^\circ C} = -105 \text{ kJ/mol}$).



Despite these potential advantages, ethane ODH has significant limitations: the need for oxygen gas requires an air separation unit (ASU) which is both capital and energy intensive (~26 kJ/mol of O_2). The mixing ethane and gaseous oxygen also creates additional safety concerns. Additionally, in order to be an attractive process, high per pass yields of ethylene have to be obtained due to the high downstream separation/purification energy costs [11].

To address these challenges, we proposed a chemical looping ODH (CL-ODH) scheme (Fig. 1) [11–14]. In this two-step process, a redox catalyst, also known as oxygen carrier, donates oxygen from its lattice to convert ethane to ethylene and water in an ODH reactor. After the redox catalyst is reduced, it is transferred to an air reactor where it is re-oxidized in air and then transferred back to the ODH reactor to complete the redox cycle. The CL-ODH process eliminates drawbacks of traditional ODH because an air separation unit is no longer needed, and the overall process is safer due to the avoidance of ethane-oxygen gas mixtures. Recent process simulations [11] indicate that the CL-ODH process can reduce energy consumption and CO_2/NO_x emissions in conventional steam cracking by as much as 87%. The significantly reduced energy consumption is largely due to the selective oxidation of hydrogen, providing energy needed for ethane dehydrogenation. Moreover, higher single-pass yield of ethylene and *in-situ* hydrogen oxidation reduces the load for the downstream purification steps. With proper design of redox catalysts to avoid over-oxidation of ethane or ethylene, the use of lattice oxygen in the redox catalyst instead of gaseous oxygen can also lead to higher ethylene selectivity [13,14].

A number of catalysts have been extensively studied for ethane ODH with oxygen co-feed [15–22], with some achieving ethylene yields over 40% when the ethane partial pressures were below 40% [23–29]. However, these active catalysts are comprised of rare metals such as tellurium, niobium, platinum and dysprosium.

Comparatively, there have been far fewer studies for CL-ODH. Recent studies investigated vanadium and molybdenum oxides as redox catalysts for CL-ODH [30–33], but these redox catalysts demonstrated

ethylene yields below 20% due to low ethane conversion (7–25%) and decreasing ethylene selectivity at higher conversions (85%–58%). Moreover, the toxicity and high cost of vanadium make it difficult for their utilization in large scale, circulating fluidized bed based CL-ODH processes.

Manganese oxides are an alternative redox catalysts that are stable at high temperatures, low-cost, and environmentally benign. Manganese based redox catalysts have been shown to be effective for chemical looping combustion (CLC) and chemical looping gasification (CLG) of methane and coal [34–40] and we have previously reported on manganese based redox catalysts for the CL-ODH of ethane [12,14,41]. In these CL-ODH studies, Mg_6MnO_8 and MnO_x/SiO_2 based redox catalysts were tested. When promoted with sodium tungstate, Mg_6MnO_8 based redox catalysts were able to achieve an ethylene yield of 68.2%, well above thermal cracking. However, MnO_x/SiO_2 based redox catalysts were not able to achieve significantly higher ethylene yields than thermal cracking. These redox catalysts were composed of distinct manganese oxide and SiO_2 phases. It is noted that manganese and silicon also form mixed oxides which may exhibit significantly different redox properties than the SiO_2 supported MnO_x investigated. Mixed Mn and Si oxides are particularly interesting for CL-ODH due to the natural abundance of manganese silicates and their environmentally benign nature. It has been reported that mixed Mn and Si Oxides can release oxygen at high temperatures with satisfactory activity and stability for chemical looping combustion [42–44]. Manganese silicates have been previously studied for the oxidative coupling of methane [45] and been utilized in processes for hydrocarbon dehydrogenation [46].

This study focuses on the development of manganese silicate redox catalysts for the ODH of ethane in a CL-ODH scheme. The effect of a sodium tungstate precursor is also investigated as a promoter as previous studies have shown it to be effective for ODH of ethane when utilized with manganese based redox catalysts due to the suppression of CO_x formation from the over oxidation of hydrocarbons [12,14]. ASPEN Plus simulations are also performed in order to compare a CL-ODH process with manganese silicate based redox catalysts with traditional steam cracking.

2. Experimental

2.1. Redox catalyst synthesis

A solid state reaction (SSR) method was used to synthesize manganese silicate particles. First, Mn_3O_4 (Noah Technologies, 99.5%) and SiO_2 (Sigma-Aldrich, 10–20 nm, 99.5%) powders were mixed together in the desired ratio for 12 h in a planetary ball mill (XBM4X, Columbia International) at a rotation speed of 250 rpm. The mixture is then pressed into pellets by a hydraulic press (YLJ-15T, MTI Corporation) at a pressure of 20 MPa. The pellets were then annealed in air in a tube furnace (GSL-1500-X50, MTI Corporation) at 1100 °C for 8 h. After annealing the particles, the particle were ground and sieved.

Three different molar ratios of Mn:Si were synthesized, 70:30, 30:70 and 05:95. A sodium tungstate promoter was added to the base redox catalyst through incipient wetness impregnation. Sodium tungstate dihydrate (Sigma Aldrich, 99.5%) was dissolved in water and then added on to the $MnSiO_x$ catalyst. Two different weight loadings were synthesized: 1.7 wt.% and 0.85 wt.% sodium. After drying overnight at 80 °C, the promoted redox catalyst was annealed in air in a tube furnace at 1100 °C for 8 h.

2.2. Ethane ODH experiments

Reaction testing was performed in a 1/4" O.D. × 1/8" I.D. quartz U-tube reactor loaded with 0.5 g of catalyst particles sieved between 425 μm and 850 μm. To hold the catalyst particles in place and reduced the gas volume of the heated reactor zone, 16 mesh white alumina grit was loaded on each side of the catalyst particles. For blank tube runs,

the entire tube was packed with the white alumina grit to maintain consistent gas residence times. The quartz U-tube was heated by a tube furnace and the gas composition and flow rate in the reactor was controlled with mass flow controllers with an automated valve manifold.

In order to determine the activity of the catalysts for the ODH of ethane, redox cycle experiments were performed. During the reduction step, the reactor environment was comprised of 80% ethane balance argon, and during the oxidation step it was changed to 17% oxygen balance argon. After each reduction and oxidation step, 100% argon was flowed into the reactor to purge any remaining gasses. The reactor gas manifold is configured such that the total flow rate into the reactor does not change between the purge and reduction steps. GHSV values were calculated assuming a 1mL catalyst bed volume. Before ODH testing, the redox catalysts were pretreated at a GHSV = 4500 h⁻¹ with 2 redox cycles comprising of a 3 min reduction step (in 80% ethane) and 3 min oxidation step (in 17% oxygen) at 900 °C to obtain a redox catalyst with stabilized chemical and physical properties. During ODH redox cycles, a GHSV of 4500 h⁻¹ or 3000 h⁻¹ and temperatures between 850 °C and 800 °C were used for testing of redox catalysts. During the reduction step, a total of 5 standard mL of ethane (with 1.25 mL argon dilution) was flown (5 s injection at GHSV = 4500 h⁻¹ and 7.5 s injection at GHSV = 3000 h⁻¹) into the reactor and the oxidation step was 3 min. The WHSV value for the reduction step was 9.64 h⁻¹ at GHSV = 4500 h⁻¹ and 6.43 h⁻¹ at GHSV = 3000 h⁻¹. The purge step between the reduction and oxidation steps was 5 min.

The products from the reduction and oxidation steps were collected in a gas sampling bag and characterized using a gas chromatograph (GC). An Agilent 7890 Series Fast RGA GC with two thermal conductivity detector (TCD) channels (He/TCD channel for CO/CO₂ analysis, Ar/TCD channel for H₂ analysis), and a flame ionization detector (FID) channel for hydrocarbon analysis was used. The system was calibrated using a refinery gas calibration standard (Agilent Part # 5190-0519). As internal standard experiments indicated insignificant coking or tar formation under the conditions tested, a carbon mass balance was used to calculate the yields. The selectivity and conversion values for carbonaceous species were calculated relative to the carbon mass balance. The total amounts of hydrogen formed and converted to water were calculated by hydrogen mass balance of all recovered species. Additional information and formulas for selectivities, yields and hydrogen conversion calculations have been included in the supplementary information.

2.3. Redox catalysts characterizations

Adsorption isotherms were collected on a Micromeritics ASAP 2010 at 77 K using N₂ as the adsorbent gas. The surface areas were evaluated using Brunauer–Emmett–Teller (BET) theory. All of the samples were degassed at 473 K under vacuum before the measurements.

Phase identification of as-prepared redox catalysts was performed using Powder X-Ray Diffraction (XRD). A Rigaku SmartLab X-ray Diffractometer with Cu K α ($\lambda = 0.1542$ nm) radiation operating at 40 kV and 44 mA. A scanning range of 10–70° (2 θ) with a step size of 0.1° holding for 3.5 s at each step was used to generate XRD patterns.

To determine the oxygen capacity, redox catalysts underwent redox cycles on a Thermal Gravimetric Analyzer (TGA, SETARAM SETSYS Evolution). As prepared catalysts were loaded into the instrument and then heated to 850 °C in a 10% O₂/90% He environment to maintain an oxidized catalyst. Next, the flow is switched to 100% He to purge oxygen and then to a 10% H₂/90% He environment to reduce the catalyst. The hydrogen is then purged and the environment is switched back to 10% O₂/90% He to re-oxidize the catalyst. A total of 20 cycles were performed and the oxygen capacity was determined from the last 3 redox cycles.

X-ray photoelectron spectroscopy (XPS) was used to analyze surface compositions and oxidation states of fresh, reduced, and cycled variants

of each of the four catalysts. For the cycled samples, redox catalyst particles that had undergone over 50 redox cycles were used. The catalysts were re-oxidized at 850 °C and then purged in an inert environment at 850 °C. The XPS system consists of a Thermo-Fisher Alpha 110 hemispherical energy analyzer, a Thermo-Fischer XR3, 300 W dual-anode X-Ray source, and an Al anode was used for all the analyses. The spectra energies were calibrated to an adventitious C1s peak of 284.6 eV.

Ethane temperature programmed reduction (TPR) experiments were conducted using the quartz U-tube reactor as described previously and QMS MKS Cirrus II. 0.5 g of catalysts (particle size of 425–850 μm) was loaded into the U-tube and then heated to 900 °C for 30 min in a 10% oxygen balance argon environment to clean and fully oxidize catalyst. After the catalyst was cooled down to room temperature in 10% oxygen, the flow was changed to 5% ethane in argon. The reactor was then heated quickly to 500 °C and held to stabilize the temperature in the reactor. The catalyst was then heated to 900 °C at a rate of 2 °C/min and held for 5 min. All of the reactor effluent was analyzed by a QMS MKS Cirrus II.

2.4. Process evaluations

ASPEN Plus® simulation was carried out using a CL-ODH model published previously [11]. Ethane conversion and product distributions from 1.7 wt.% Na promoted redox catalyst (Mn:Si = 70:30) were used in the model to estimate the process performance using the promoted Si-Mn redox catalyst. The performance of the CL-ODH process was then compared with that of a reference steam-cracking process. Further details with respect to the ASPEN model and simulation can be found in the reference and the supplemental file [11].

3. Results and discussion

3.1. Redox catalyst characterization

XRD patterns of the as prepared manganese silicate redox catalysts are shown in Fig. 2. For all the redox catalysts, characteristic peaks of the Mn₇SiO₁₂ phase (PDF# 04-008-9539) and the α-cristobalite phase (PDF# 04-008-7641) were detected. Promoted redox catalysts also showed the cubic Na₂WO₄ phase (PDF# 04-008-8508). It can be seen that as the Mn content increases, the intensity of peaks associated with Mn₇SiO₁₂ increases and peaks associated with SiO₂ decrease in intensity. The α-cristobalite phase that is detected by XRD is likely to be excess α-cristobalite that is not converted into Mn₇SiO₁₂. XRD patterns of redox catalysts after reaction testing can be found in the supplementary information (Fig. S5). BET analysis indicated that the surface areas for all the base redox catalysts were less than 1 m²/g.

Oxygen capacity values, determined from the % of mass lost during H₂ – O₂ redox cycling in the TGA, are summarized in Table 1. As the ratio of Mn:Si increased, the oxygen capacity of the redox catalyst also increased. These results indicate that the Mn₇SiO₁₂ phase is primarily responsible for oxygen donation during the reduction step. When the rate of oxygen loss/donation was calculated as in a previous study [12], the rate of oxygen loss of the Mn:Si = 70:30 redox catalyst (Fig. S1) was lower than Mg₆MnO₈ redox catalysts, but higher than Mn/SiO₂ redox catalysts. The maximum oxygen donation rate for Mn:Si = 70:30 was ~3%/min (Fig. S1), 0.8%/min for Mn/SiO₂ and 7%/min for Mg₆MnO₈ (reported in our previous study).

3.2. ODH reaction testing

In order to determine the ODH performance of the un-promoted redox catalysts, they were tested at 850 °C under a GHSV of 4500 h⁻¹. A blank (thermal cracking) experiment was also performed for comparison (Table 2). A more detailed product breakdown can be found in the supplementary information. Reaction testing indicates that the presence

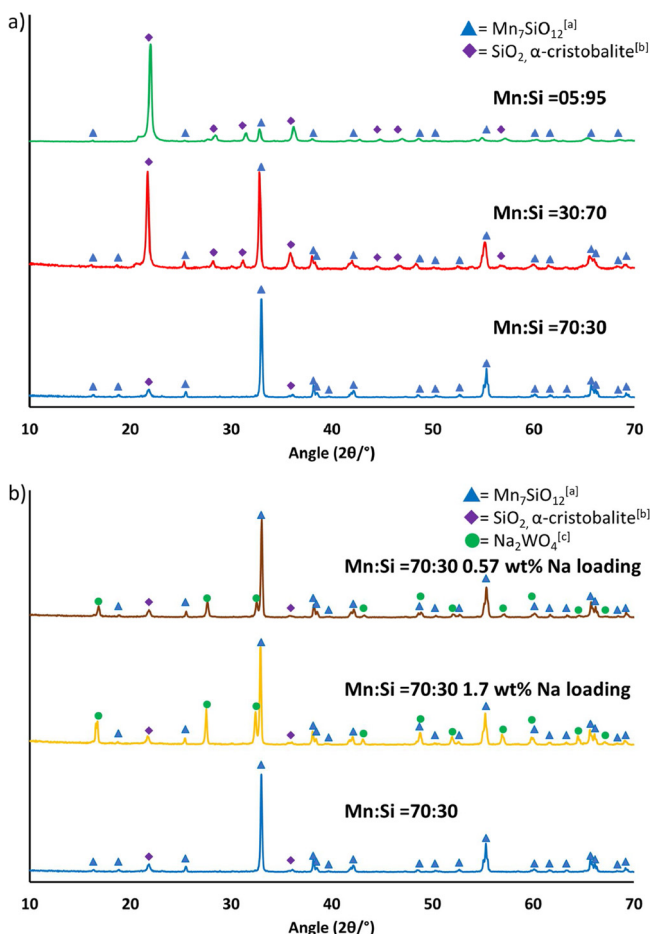


Fig. 2. XRD patterns of as-prepared redox catalysts (a) un-promoted redox catalysts at three different Mn:Si ratios: 05:95, 30:70 and 70:30; (b) un-promoted and promoted (1.7 wt.%, 0.57 wt.% Na) redox catalysts with Mn:Si = 70:30. [a]PDF# 04-008-9539 [b] PDF# 04-008-7641 [c]PDF#04-008-8508.

Table 1
Oxygen capacity for redox catalysts.

Redox Catalyst	Oxygen Capacity (%)
Mn:Si = 70:30	5.84%
Mn:Si = 30:70	1.94%
Mn:Si = 05:95	0.41%

Table 2
ODH reaction data at 850 °C and GHSV = 4500 h⁻¹.

Catalyst	Ethane Conversion	Ethylene Selectivity	CO _x selectivity	H ₂ conversion
Blank	62.87%	89.95%	0.00%	0.00%
Mn:Si = 70:30	80.51%	57.10%	33.70%	95.29%
Mn:Si = 30:70	66.57%	84.91%	4.09%	52.95%
Mn:Si = 05:95	64.19%	88.07%	1.36%	24.11%
Mn:Si = 70:30 – Na ₂ WO ₄ (1.7 wt.% Na)	67.15%	86.66%	1.93%	74.06%
Mn:Si = 70:30 – Na ₂ WO ₄ (0.57 wt.% Na)	69.41%	83.68%	3.73%	88.16%

of a redox catalyst improves ethane conversion when compared to thermal cracking for all Mn:Si ratios. While the Mn:Si = 70:30 redox catalyst exhibit the lowest ethylene yield (45.97%) and highest CO_x

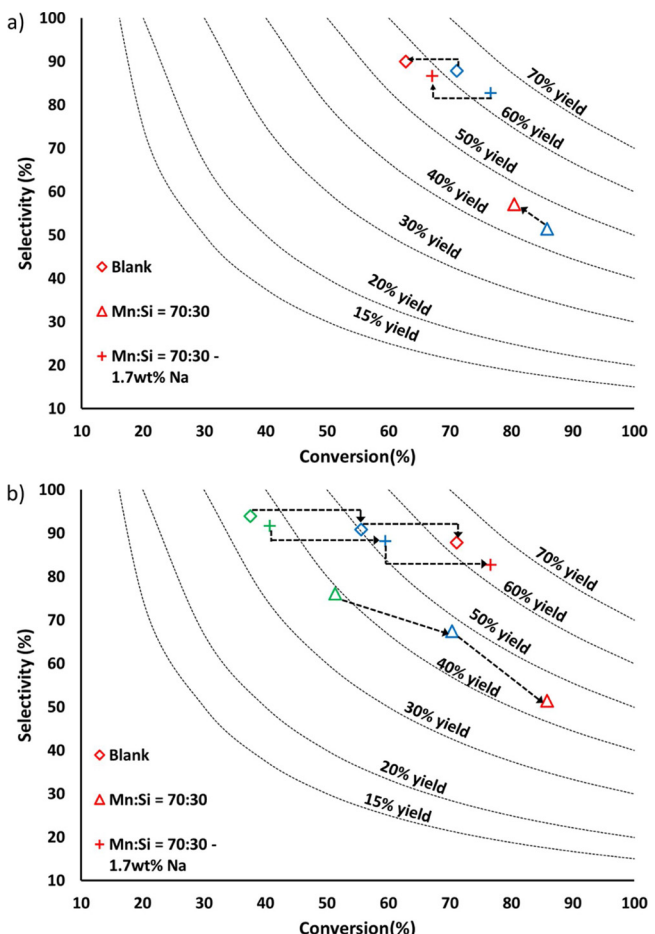


Fig. 3. ODH reaction data (a) at varying GHSV (Blue: 3000 h⁻¹, Red: 4500 h⁻¹ and 850 °C) b) at varying temperatures (Green: 800 °C, Blue: 825 °C, Red: 850 °C and GHSV = 3000 h⁻¹). Arrows point in direction of increasing GHSV or temperature. (For interpretation of the references to colour in this figure legend, the reader is referred to the web version of this article.)

selectivity (33.70%) of all the un-promoted redox catalysts, it has a significantly higher H₂ conversion (95.29% vs. 52.95% and 22.77%). The conversion of H₂ to water helps push the equilibrium of ethane ODH forward as well as generate heat for the overall CL-ODH process. Previous studies have determined that a H₂ conversion of 70% is desired for the CL-ODH process from a heat balance standpoint [11] and the addition of Na₂WO₄ as a promoter has been previously shown to lower H₂ conversion [12,14]. Therefore, we chose the Mn:Si = 70:30 redox catalyst to be promoted with Na₂WO₄ as it has the highest H₂ conversion value and the highest oxygen carrying capacity.

After promotion with Na₂WO₄ at two different loadings (1.7% and 0.57 wt.% Na), the CO_x selectivity decreased significantly. The 1.7 wt.% Na promoted redox catalyst had a lower CO_x selectivity (1.93% vs. 3.73%) and H₂ conversion (74.06% vs. 88.16%) and a slightly higher ethylene yield (58.2% vs. 58.1%). These results indicate that the 1.7 wt.% Na promoted redox catalyst is superior due to its higher ethylene yield, lower CO_x selectivity while still converting more than 70% of the hydrogen produced during the ODH reaction.

Further reaction testing was done on the un-promoted and 1.7 wt.% Na promoted Mn:Si = 70:30 redox catalyst to test the effects of GHSV (Fig. 3a) and temperature (Fig. 3b). A more detailed product breakdown can be found in the supplementary information file. It can be seen that the promoted redox catalyst has a higher ethylene yield than the un-promoted redox catalyst and thermal cracking under all the tested conditions. As expected, a decrease in GHSV led to an increase in ethane conversion and a decrease in ethylene selectivity. The 1.7 wt.%

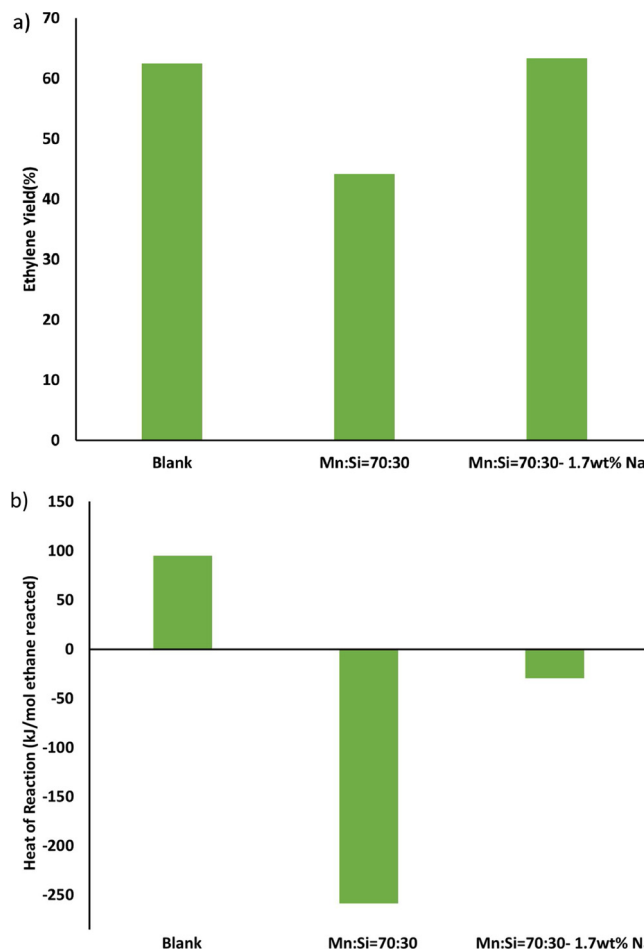


Fig. 4. Comparison of a) ethylene yield and b) Overall heat of reaction for each mole of ethane passing through the reactor considering the actual product yields. (Temperature = 850 °C, GHSV of 3000 h⁻¹).

Na promoted redox catalysts had the smaller drop in ethylene selectivity (86.66%–82.64%) than the un-promoted redox catalysts (57.10%–51.35%) when the GHSV was decreased from 4500 h⁻¹ to 3000 h⁻¹. A decrease in GHSV leads to an increase in gas residence time, which can promote the sequential combustion of ethylene products. With decreasing reaction temperature, the ethane conversion also decreases while the ethylene selectivity increases. The 1.7wt% Na promoted redox catalyst exhibited a smaller selectivity drop (91.64%–82.64%) than the un-promoted redox catalyst (76.1%–51.35%) as the temperature increased from 800 °C to 850 °C. At all temperature and GHSV conditions, the 1.7 wt.% Na promoted redox catalyst had a higher ethylene yield than the un-promoted redox catalysts and thermal blank.

While there is a large increase in the ethylene yield between the un-promoted and 1.7 wt.% Na promoted redox catalyst (30.4% at 850 °C and GHSV of 3000 h⁻¹), the ethylene yield of the blank sample is only slightly less than the 1.7 wt.% Na promoted redox catalyst (1.4% at 850 °C and GHSV of 3000 h⁻¹). However there is a significant difference in the overall heat of reaction between the blank, un-promoted and 1.7 wt.% Na promoted redox catalyst (Fig. 4). The blank sample has an endothermic heat of reaction (94.9 kJ/mol ethane each pass), both redox catalysts lead to exothermic overall heats of reaction [-258.5(un-promoted) and -29.2(1.7 wt.% Na promoted) kJ/mol ethane each pass]. The exothermicity for both redox catalysts is due to the combustion of hydrogen and hydrocarbons (CO_x formation). This means that in the blank (thermal cracking) case, heat would need to be provided to maintain the temperature for thermal cracking. In comparison, CL-ODH using these redox catalysts can allow authothermal

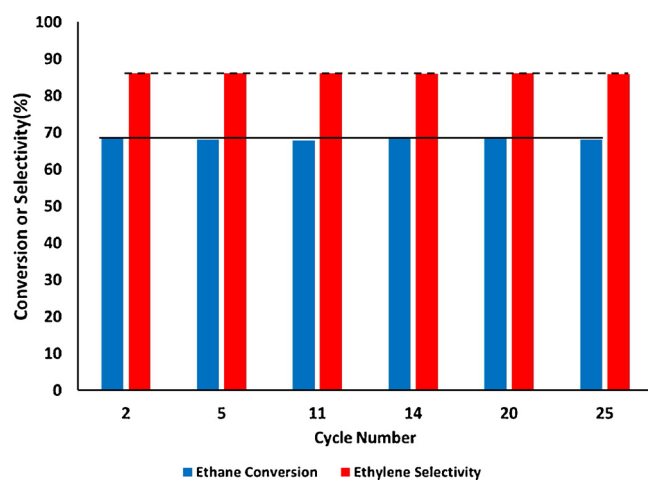


Fig. 5. 25 cycle Ethane ODH data for 1.7 wt.% Na promoted redox catalyst.

operations. Further details with respect to the benefit of the auto-thermal CL-ODH reactions are provided in the ASPEN Plus® simulation section.

It is important for a redox catalyst in the proposed CL-ODH scheme to remain stable for an extended number of redox cycles. A 25 cycled redox test shows no deactivation or loss in selectivity for the 1.7 wt.% Na promoted redox catalyst, indicating that its performance is stable over these 25 redox cycles (Fig. 5).

3.3. Ethane temperature programmed reaction

In order to study the ODH reaction pathway over the manganese silicate redox catalysts, ethane TPR were performed. The discussion below will focus on the blank, un-promoted and 1.7 wt.% Na promoted Mn:Si = 70:30 redox catalysts. Mass spectra of mass 26 (ethylene), 44 (carbon dioxide), and 18 (water) from the TPR experiments are shown in Fig. 6. Mass spectra of Mass 30 (ethane) can be found in Fig. S2. For the thermal blank, the only mass detected during the TPR experiment was mass 26, due to the lack of available oxygen in the sample. The onset temperature for ethylene production was 775 °C, which corresponds with thermal cracking temperatures of ethane. The un-promoted redox catalyst showed an ethane conversion onset temperature of ~625 °C, well below thermal cracking temperatures. The deep oxidation of ethane led to the production of carbon dioxide and water which was followed by ethylene production (onset temperature of 700 °C). On the 1.7 wt.% Na promoted redox catalyst, the onset temperature for carbon dioxide, water, and ethylene were all similar to thermal cracking. As reported in previous work on sodium tungstate promoted manganese based redox catalysts [14], the sodium tungstate promoter suppresses the over oxidation of ethane/ethylene through the inhibition of ethane activation on the surface. While both redox catalysts are active for hydrogen combustion, the un-promoted redox catalyst is also active for the deep oxidation of ethane and ethylene, leading to higher ethane conversion and lower ethylene selectivity.

3.4. Surface characterizations

XPS analysis was performed to determine the nature of surface manganese and silicon species on the redox catalysts. The three redox catalysts studied were the un-promoted, 1.7 wt.% Na, and 0.57 wt.% Na redox catalysts (Mn:Si = 70:30). For each of these redox catalysts, we analyzed two different variations: as-prepared and cycled redox catalysts (undergone more than 50 redox cycles ending in oxidation and cooled under an inert environment). In Table 3, the near-surface atomic composition (normalized, carbon and oxygen free basis) for all the redox catalysts analyzed are summarized. On both as-prepared un-

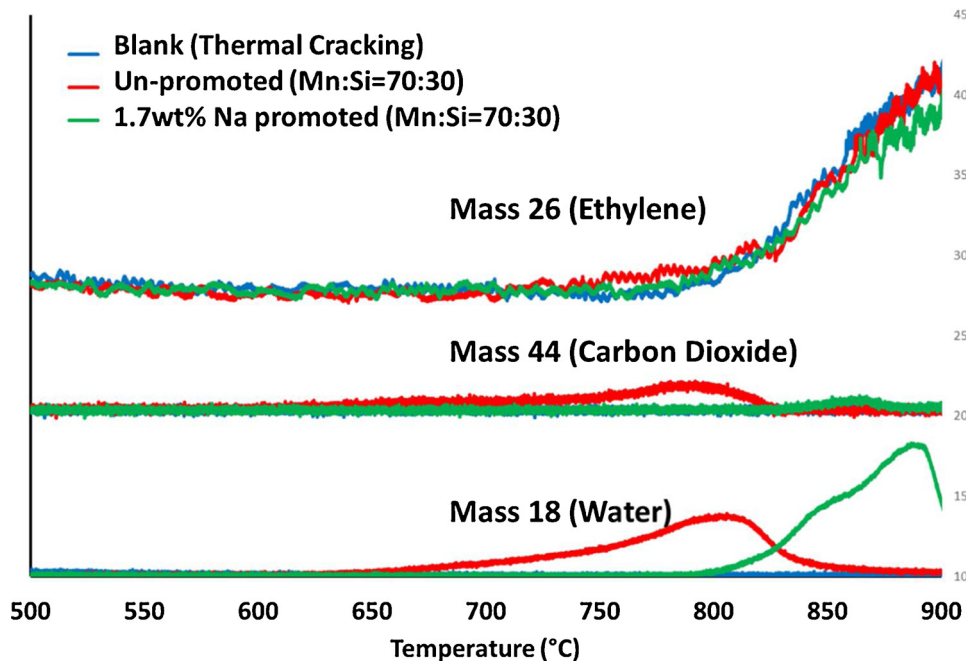


Fig. 6. Ethane TPR results for Mass 26(ethylene), Mass 18(water), and Mass 44 (carbon dioxide).

Table 3

Near-surface atomic % on as-prepared and cycled catalysts (oxygen and carbon free basis).

Catalyst	Mn%	Si%	Na%	W%
Un-promoted: as-prepared	27.09	72.91	0	0
Un-promoted: cycled	33.84	66.16	0	0
1.7 wt.% Na promoted: as-prepared	21.00	51.47	18.35	9.19
1.7 wt.% Na promoted: cycled	35.49	43.94	13.65	6.92
0.57 wt.% Na promoted: as-prepared	27.73	60.80	8.27	3.21
0.57 wt.% Na promoted: cycled	29.66	56.47	9.91	3.96

promoted and promoted redox catalysts, it can be seen that there is a significant enrichment of Si as compared to Mn:Si ratio of the bulk base redox catalyst. There is also an enrichment of sodium on the promoted redox catalysts similar to the enrichment found on sodium tungstate promoted Mg_6MnO_8 [14]. The as-prepared Na enrichment factor (observed surface Na% divided by the bulk Na%) is 3.69 for the 1.7 wt.% Na promoted redox catalyst and 4.75 for the 0.57 wt.% Na promoted redox catalyst. The ratio of Na to W on the as-prepared promoted redox catalysts is about 2, as found in sodium tungstate. After cycling, there is a slight enrichment of Mn and loss of Si on the near-surface of both un-promoted and promoted redox catalysts. For the 1.7 wt.% Na promoted redox catalyst, there is a small decrease of both Na and W after cycling, decreasing the Na enrichment factor to 2.75. However, on the 0.57 wt.% Na promoted redox catalyst there is a slight enrichment of both Na and W increasing its Na enrichment factor to 5.70. These results indicate that i) tungsten is able to retain sodium on the surface of the catalyst and can cooperate with alkali species to suppress deep oxidation of hydrocarbons [14,47–49] and ii) there is an enrichment of sodium tungstate on the surface of the redox catalyst. DSC runs on the 1.7 wt.% Na promoted redox catalyst show a melting behavior at 650 °C, likely corresponding to the melting of Na_2WO_4 which has a bulk melting temperature of 698 °C. These results along with XPS surface analysis indicate that the Na_2WO_4 forms a physical layer on the near surface of the catalyst and this layer may be molten at the reaction conditions.

Analysis of the Si 2p peak on both the fresh and cycled redox catalysts can be seen in Fig. 7. On all as-prepared redox catalysts (Fig. 7a), peaks associated with SiO_2 species (cristobalite and/or quartz) [50] and

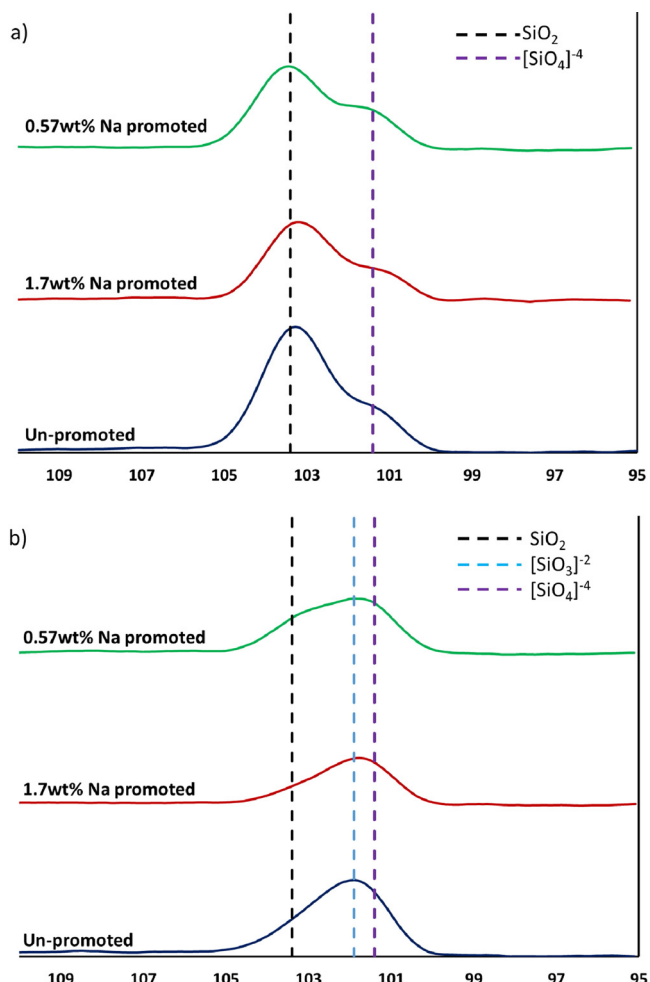


Fig. 7. XPS spectra of Si 2p peaks of a) as-prepared and b) cycled redox catalysts.

Table 4
 ΔeV of Mn 3s multiplet peaks for as-prepared and cycled redox catalysts.

Catalyst	Mn 3s ΔeV
Un-promoted: as-prepared	5.3
Un-promoted: cycled	5.9
1.7 wt.% Na promoted: as-prepared	5.4
1.7 wt.% Na promoted: cycled	5.8
0.57 wt.% Na promoted: as-prepared	5.4
0.57 wt.% Na promoted: cycled	6.2

the orthosilicate($[\text{SiO}_4]^{-4}$) mixed oxides [50,51] were found. The SiO_2 type species is consistent with the α -cristobalite phase observed in XRD (Fig. 2) and/or an amorphous silica phase. The ortho-silicate type species is completely consistent with $\text{Mn}_7\text{SiO}_{12}$, although the presence of XRD insensitive Mn_2SiO_4 surface species cannot be entirely dismissed. On the cycled redox catalysts (Fig. 7b), it can be seen that there was decrease in the overall Si 2p peak binding energy from 103.2 eV to 101.9 eV. Peaks associated with SiO_2 species were found again, but their relative intensity decreased. The orthosilicate type peak is still present consistent with unreduced $\text{Mn}_7\text{SiO}_{12}$. There is also a new peak consistent with the $[\text{SiO}_3]^{-2}$ ions [51]. XRD of the cycled samples (Fig. S5) support assignment of this peak to MnSiO_3 . This is consistent with reports that during oxygen is released from $\text{Mn}_7\text{SiO}_{12}$, SiO_2 is consumed to form MnSiO_3 [52].

The Mn 3s spectrum has been previously used to distinguish manganese oxidation states [53]. The Mn 3s spectrum has two multiplet peaks caused by the coupling of non-ionized 3s electrons with 3d valence band electrons. The ΔeV between the two peaks on the Mn 3s spectrum can be used to estimate the average oxidation state of manganese. As the average oxidation state decreases, the ΔeV increases. This value for each of the tested redox catalysts can be found in Table 4. For all of the as-prepared redox catalysts, the ΔeV between the two multiplet peaks are all ~ 5.4 eV which corresponds to an average oxidation state between 2+ and 3+ [54]. After cycling, the ΔeV value increases to ~ 6.0 eV for all redox catalysts, indicating decreasing oxidation state. Spectra on the Mn 3s peaks can be found in the supplementary information (Figs. S3 and S4).

While it is difficult to distinguish between the Mn^{2+} and Mn^{3+} oxidation states from the Mn 2p spectra due to their similar peak positions [55], the Mn 2p peak can also be used in addition to the Mn 3s peak to gain insight into the valence state of manganese. In Fig. 8, the Mn 2p spectra are shown for all of the as-prepared and cycled redox catalysts. There were no significant differences in the peaks between the different redox catalysts; the overall Mn 2p 3/2 peak position was

between 641.3 and 641.4 eV. However there is a small feature on the cycled redox catalysts at ~ 647 eV that is not present of the as-prepared catalysts. This is consistent with a satellite peak for Mn^{2+} [55] and the presence of MnSiO_3 . In contrast to the to the previously studied Mg_6MnO_8 redox catalysts [14], the lack of a high binding energy shoulder for the Mn 2p 3/2 peak indicates a lack of near surface Mn^{4+} species on the manganese silicate redox catalysts. On Mg_6MnO_8 redox catalysts, as the presence of Mn^{4+} on the near surface of the redox catalyst was associated with deep oxidation [14]. Its absence on the un-promoted manganese silicate redox catalyst is consistent with the improved ethylene selectivity of the un-promoted manganese silicate as compared to un-promoted Mg_6MnO_8 (51.4% vs. 17.9%). However, since all cycled manganese silicate redox catalysts have similar oxidation states, the average oxidation state was not the primary factor in determine the selectivity of the catalyst. Instead, the sodium tungstate promoter is likely to act as a physical blocker, suppressing the surface activation of ethane and ethylene and the over oxidation to CO_x species.

3.5. Process analysis and practical implications

The performance of the CL-ODH process is determined using the ASPEN Plus® simulator and is compared with traditional steam cracking, based on the models developed in our previous work [11]. The product distribution for CL-ODH, based on the results from the 1.7 wt.% Na promoted redox catalyst (see Table S2) is used for the simulation, whereas data from literature is used for steam cracking [2]. The ASPEN Plus® modules, property methods, and physical property databanks are summarized in Table S3 and the flowsheet for the CL-ODH process is shown in Fig. S6. Owing to the selective combustion of H_2 product, the reactor-regenerator scheme of the CL-ODH is net exothermic, unlike the steam cracking process, which requires all overall energy input of 15.2 GJ_{Th}/tonne ethylene. Overall, the CL-ODH with the promoted Mn-Si redox catalyst requires 1.7 GJ_{Th} of energy for each tonne of ethylene produced. This corresponds to 89% less energy demand compared to steam cracking. The primary energy saving is resulted from the ethane conversion step, which is net exothermic as compared to the highly endothermic cracking process. In addition, 38% decrease in compression work is projected for downstream separations. Comparisons for the energy distributions of the two processes are depicted in Fig. 9. Compared to steam cracking, the CL-ODH can result in 89% reduction in the CO_2 and NO_x emissions, which is proportional to its energy savings. As shown in Fig. S7, the cracking process has an energy deficiency of 1.42 GJ_{Th}/tonne ethylene even after all the fuel gas produced in the process (CO , H_2 and CH_4) are combusted. The CL-ODH, on the other hand, has an excess fuel equivalent to roughly 5 GJ_{Th}/tonne ethylene. These results highlight the potential advantages and benefits

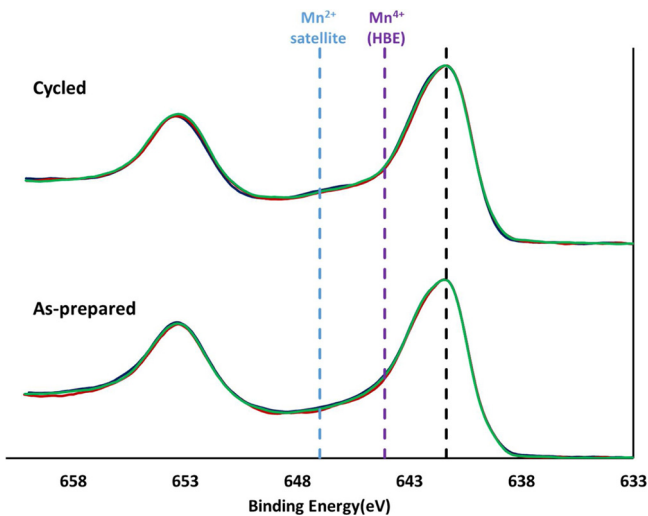


Fig. 8. XPS spectra of Mn 2p peaks of as-prepared and cycled of all redox catalysts.

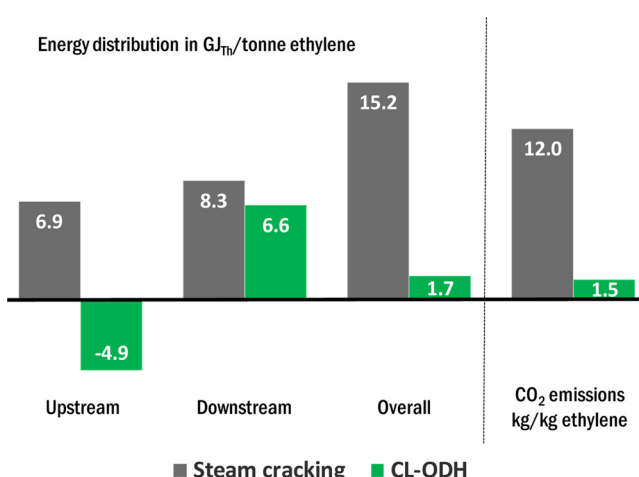


Fig. 9. Energy and emission comparison between steam cracking and CL-ODH.

of CL-ODH using the Mn-Si based redox catalysts.

4. Conclusion

The current study investigated manganese silicates as redox catalysts for the oxidative dehydrogenation of ethane in a chemical looping scheme. Redox catalysts with different molar ratios of Mn:Si were synthesized. Characterization of the redox catalysts indicated the presence of $\text{Mn}_7\text{SiO}_{12}$ and SiO_2 phases. The Mn:Si = 70:30 redox catalyst was the preferred base redox catalyst due its high oxygen carrying capacity and H_2 conversion, despite its relatively high CO_x selectivity (36.52% at 3000 h^{-1} GHSV and 850 °C). When promoted with sodium tungstate, the ethylene yield increased significantly (44.08%–63.33%) while CO_x selectivity decreased (36.52%–2.96% at 3000 h^{-1} GHSV and 850 °C). Ethane TPR indicated that the sodium tungstate promoter suppresses the over oxidation of ethane and ethylene and decreases the redox catalyst's ability to activate ethane.

XPS analysis of the redox catalysts indicated an enrichment of sodium and tungstate on the near surface of the sodium tungstate promoted redox catalysts, and DSC experiments show the melting of sodium tungstate ~200 °C below reaction conditions. These results indicate that a molten layer of sodium tungstate is likely to present on the surface of the redox catalyst and physically block the sites for ethane and ethylene activation and hence CO_x formation as previously seen in oxidative coupling of methane processes [56]. Analysis of Si spectra indicated that as-prepared redox catalysts are consisted of α -cristobalite and $\text{Mn}_7\text{SiO}_{12}$ phases. After cycling, the $\text{Mn}_7\text{SiO}_{12}$ phase is partially reduced and reacts with SiO_2 to form MnSiO_3 . Analysis of Mn spectra indicated an absence of near surface Mn^{4+} , which was attributed to the low ethylene selectivity for Mg_6MnO_8 based redox catalysts in our previous study [14]. ASPEN Plus® simulations indicated that the CL-ODH process with sodium tungstate promoted manganese silicate redox catalysts has the potential to reduce the energy demand and CO_2/NO_x emissions for ethylene production by as much as 89% when compared to commercial steam cracking. The effectiveness of sodium tungstate as a promoter and the enrichment of sodium tungstate near the surface of the redox catalyst observed in this study also warrant further studies into the nature and effects of the sodium tungstate promoter on manganese silicate based redox catalysts.

Acknowledgements

We acknowledge the funding support from Advanced Research Project Agency-Energy (ARPA-E) of the US Department of Energy (DR-AR0000327), the U.S. National Science Foundation (Award No. CBET-1604605) and the Kenan Institute of Engineering, Technology, and Science at NC State University. We also acknowledge the assistance of Mr. Petr Novotny at North Carolina State University for XPS measurements. The correspondence author of this publication consults for EcoCatalytic Technologies on oxidative dehydrogenation of ethane. The author also conducts research in areas of interest similar to the business interests of EcoCatalytic Technologies. The terms of this arrangement have been reviewed and approved by NC State University in accordance with its policy on objectivity in research.

Appendix A. Supplementary data

Supplementary material related to this article can be found, in the online version, at doi: <https://doi.org/10.1016/j.apcatb.2018.03.037>.

References

- [1] Technology Roadmap- Energy and GHG Reductions in the Chemical Industry via Catalytic Processes, International Energy Agency, 2013, pp. 1–60.
- [2] Ullmann's Encyclopedia of Industrial Chemistry, Wiley-VCH Verlag GmbH & Co. KGaA, Weinheim, Germany, 2000.
- [3] T. Ren, M. Patel, K. Blok, Olefins from conventional and heavy feedstocks: energy use in steam cracking and alternative processes, *Energy* 31 (2006) 425–451, <http://dx.doi.org/10.1016/j.energy.2005.04.001>.
- [4] J.J.H.B. Sattler, J. Ruiz-Martinez, E. Santillan-Jimenez, B.M. Weckhuysen, Catalytic dehydrogenation of light alkanes on metals and metal oxides, *Chem. Rev.* 114 (2014) 10613–10653, <http://dx.doi.org/10.1021/cr5002436>.
- [5] C.A. Gärtner, A.C. van Veen, J.A. Lercher, Oxidative dehydrogenation of ethane: common principles and mechanistic aspects, *ChemCatChem* 5 (2013) 3196–3217, <http://dx.doi.org/10.1002/cctc.201200966>.
- [6] M.M. Bhasin, Is true ethane oxydehydrogenation feasible? *Top. Catal.* 23 (2003) 145–149, <http://dx.doi.org/10.1023/A:1024884623238>.
- [7] R. Burch, R. Swarnakar, Oxidative dehydrogenation of ethane on vanadium-molybdenum oxide and vanadium-niobium-molybdenum oxide catalysts, *Appl. Catal.* 70 (1991) 129–148, [http://dx.doi.org/10.1016/S0166-9834\(00\)84159-7](http://dx.doi.org/10.1016/S0166-9834(00)84159-7).
- [8] E.A. Mamedov, V. Cortés Corberán, Oxidative dehydrogenation of lower alkanes on vanadium oxide-based catalysts. The present state of the art and outlooks, *Appl. Catal. A Gen.* 127 (1995) 1–40, [http://dx.doi.org/10.1016/0926-860X\(95\)00056-9](http://dx.doi.org/10.1016/0926-860X(95)00056-9).
- [9] M.A. Bañares, Supported metal oxide and other catalysts for ethane conversion: a review, *Catal. Today* 51 (1999) 319–348, [http://dx.doi.org/10.1016/S0920-5861\(99\)00053-X](http://dx.doi.org/10.1016/S0920-5861(99)00053-X).
- [10] S. Gaab, J. Find, T.E. Müller, J.A. Lercher, Kinetics and mechanism of the oxidative dehydrogenation of ethane over Li/Dy/Mg/O(Cl) mixed oxide catalysts, *Top. Catal.* 46 (2007) 101–110, <http://dx.doi.org/10.1007/s11244-007-0320-x>.
- [11] V.P. Haribal, L.M. Neal, F. Li, Oxidative dehydrogenation of ethane under a cyclic redox scheme – process simulations and analysis, *Energy* 119 (2017) 1024–1035, <http://dx.doi.org/10.1016/j.energy.2016.11.039>.
- [12] L.M. Neal, S. Yusuf, J.A. Sofranko, F. Li, Oxidative dehydrogenation of ethane: a chemical looping approach, *Energy Technol.* 4 (2016) 1200–1208, <http://dx.doi.org/10.1002/ente.201600074>.
- [13] Y. Gao, L.M. Neal, F. Li, Li-promoted $\text{LaSr}_2\text{xFeO}_4\text{-}\delta$ core-shell redox catalysts for oxidative dehydrogenation of ethane under a cyclic redox scheme, *ACS Catal.* 6 (2016) 7293–7302, <http://dx.doi.org/10.1021/acscatal.6b01399>.
- [14] S. Yusuf, L.M. Neal, F. Li, Effect of promoters on manganese-containing mixed metal oxides for oxidative dehydrogenation of ethane via a cyclic redox scheme, *ACS Catal.* 7 (2017) 5163–5173, <http://dx.doi.org/10.1021/acscatal.7b02004>.
- [15] M. Abello, M. Gomez, O. Ferretti, $\text{Mo}/\gamma\text{-Al}_2\text{O}_3$ catalysts for the oxidative dehydrogenation of propane, *Appl. Catal. A Gen.* 207 (2001) 421–431, [http://dx.doi.org/10.1016/S0926-860X\(00\)00680-3](http://dx.doi.org/10.1016/S0926-860X(00)00680-3).
- [16] E. Heraclous, M. Machli, A.A. Lemonidou, I.A. Vasalos, Oxidative dehydrogenation of ethane and propane over vanadia and molybdena supported catalysts, *J. Mol. Catal. A Chem.* 232 (2005) 29–39, <http://dx.doi.org/10.1016/j.molcata.2005.01.027>.
- [17] B. Solana, A. Dejoz, T. Garcia, P. Concepcion, J. Nieto, M. Vazquez, M. Navarro, Molybdenum–vanadium supported on mesoporous alumina catalysts for the oxidative dehydrogenation of ethane, *Catal. Today* 117 (2006) 228–233, <http://dx.doi.org/10.1016/j.cattod.2006.05.025>.
- [18] H. Zhu, D.C. Rosenfeld, D.H. Anjum, V. Caps, J.-M. Basset, Green synthesis of Ni-Nb oxide catalysts for low-temperature oxidative dehydrogenation of ethane, *ChemSusChem* 8 (2015) 1254–1263, <http://dx.doi.org/10.1002/cssc.201403181>.
- [19] L. Ji, J. Liu, Excellent promotion by lithium of a lanthanum–calcium oxide catalyst for oxidative dehydrogenation of ethane to ethene, *Chem. Commun.* (1996) 1203, <http://dx.doi.org/10.1039/cc9960001203>.
- [20] B. Fu, J. Lu, P.C. Stair, G. Xiao, M.C. Kung, H.H. Kung, Oxidative dehydrogenation of ethane over alumina-supported Pd catalysts. Effect of alumina overlayer, *J. Catal.* 297 (2013) 289–295, <http://dx.doi.org/10.1016/j.jcat.2012.10.023>.
- [21] H.H. Kristoffersen, H. Metiu, Molten LiCl layer supported on MgO: its possible role in enhancing the oxidative dehydrogenation of ethane, *J. Phys. Chem. C* 119 (2015) 8681–8691, <http://dx.doi.org/10.1021/jpc528628>.
- [22] C.A. Gärtner, A.C. van Veen, J.A. Lercher, Oxidative dehydrogenation of ethane on dynamically rearranging supported chloride catalysts, *J. Am. Chem. Soc.* 136 (2014) 12691–12701, <http://dx.doi.org/10.1021/ja505411s>.
- [23] J.M.L. Nieto, P. Botella, P. Concepción, A. Dejoz, M.I. Vázquez, Oxidative dehydrogenation of ethane on Te-containing MoVNbO catalysts, *Catal. Today* (2004) 241–245, <http://dx.doi.org/10.1016/j.cattod.2004.03.040>.
- [24] P. Botella, E. García-González, A. Dejoz, J.M. López Nieto, M.I. Vázquez, J. González-Calbet, Selective oxidative dehydrogenation of ethane on MoVTNbO mixed metal oxide catalysts, *J. Catal.* 225 (2004) 428–438, <http://dx.doi.org/10.1016/j.jcat.2004.04.024>.
- [25] Q. Xie, L. Chen, W. Weng, H. Wan, Preparation of MoVTNbO mixed oxide catalysts using a slurry method for selective oxidative dehydrogenation of ethane, *J. Mol. Catal. A Chem.* 240 (2005) 191–196, <http://dx.doi.org/10.1016/j.molcata.2005.07.004>.
- [26] C.P. Kumar, S. Gaab, T.E. Müller, J.A. Lercher, Oxidative dehydrogenation of light alkanes on supported molten alkali metal chloride catalysts, *Top. Catal.* 50 (2008) 156–167, <http://dx.doi.org/10.1007/s11244-008-9102-3>.
- [27] B. Tope, Y. Zhu, J.A. Lercher, Oxidative dehydrogenation of ethane over $\text{Dy}_2\text{O}_3/\text{MgO}$ supported LiCl containing eutectic chloride catalysts, *Catal. Today* 123 (2007) 113–121, <http://dx.doi.org/10.1016/j.cattod.2007.02.020>.
- [28] A.S. Bodke, D. Henning, L.D. Schmidt, S.S. Bharadwaj, J.J. Maj, J. Siddall, Oxidative dehydrogenation of ethane at millisecond contact times: effect of H_2 addition, *J. Catal.* 191 (2000) 62–74, <http://dx.doi.org/10.1006/jcat.1999.2802>.
- [29] A.S. Bodke, D.A. Olschki, L.D. Schmidt, E. Ranzi, High selectivities to ethylene by partial oxidation of ethane, *Science* (80-) 285 (1999) 712–715, <http://dx.doi.org/10.1126/science.285.5428.712>.
- [30] S. Al-Ghamdi, M. Volpe, M.M. Hossain, H. de Lasa, VOx/c-Al2O3 catalyst for

oxidative dehydrogenation of ethane to ethylene: desorption kinetics and catalytic activity, *Appl. Catal. A Gen.* 450 (2013) 120–130, <http://dx.doi.org/10.1016/j.apcata.2012.10.007>.

[31] A.H. Elbadawi, M.S. Ba-Shammakh, S. Al-Ghamdi, S.A. Razzak, M.M. Hossain, Reduction kinetics and catalytic activity of VO_x/γ-Al₂O₃-ZrO₂ for gas phase oxygen free ODH of ethane, *Chem. Eng. J.* 284 (2016) 448–457, <http://dx.doi.org/10.1016/j.cej.2015.08.048>.

[32] S.N. Khadzhiev, N.Y. Usachev, I.M. Gerzeliev, E.P. Belanova, V.P. Kalinin, V.V. Kharlamov, A.V. Kazakov, S.A. Kanaev, T.S. Starostina, A.Y. Popov, Oxidative dehydrogenation of ethane to ethylene in a system with circulating microspherical metal oxide oxygen carrier: 1. Synthesis and study of the catalytic system, *Pet. Chem.* 55 (2015) 651–654, <http://dx.doi.org/10.1134/S0965544115080125>.

[33] S.N. Khadzhiev, N.Y. Usachev, I.M. Gerzeliev, V.P. Kalinin, V.V. Kharlamov, E.P. Belanova, A.V. Kazakov, S.A. Kanaev, T.S. Starostina, Ethane conversion involving lattice oxygen of oxide systems, *Pet. Chem.* 55 (2015) 640–644, <http://dx.doi.org/10.1134/S0965544115080113>.

[34] T. Mattisson, T. Mattisson, Materials for chemical-looping with oxygen uncoupling, *ISRN Chem. Eng.* 2013 (2013) 1–19, <http://dx.doi.org/10.1155/2013/526375>.

[35] A. Shafiefarhood, A. Stewart, F. Li, Iron-containing mixed-oxide composites as oxygen carriers for Chemical Looping with Oxygen Uncoupling (CLOU), *Fuel* 139 (2015) 1–10, <http://dx.doi.org/10.1016/j.fuel.2014.08.014>.

[36] A. Shafiefarhood, J. Zhang, L.M. Neal, F. Li, M. Uenishi, M. Kimura, T. Okamoto, N. Hamada, T.-L. Hsieh, A. Tong, Z. Sun, L.-S. Fan, Rh-promoted mixed oxides for “low-temperature” methane partial oxidation in the absence of gaseous oxidants, *J. Mater. Chem. A* 5 (2017) 11930–11939, <http://dx.doi.org/10.1039/C7TA01398A>.

[37] V.P. Haribal, F. He, A. Mishra, F. Li, Iron-doped BaMnO₃for hybrid water splitting and syngas generation, *ChemSusChem* 10 (2017) 3402–3408, <http://dx.doi.org/10.1002/cssc.201700699>.

[38] A. Mishra, N. Galinsky, F. He, E.E. Santiso, F. Li, Perovskite-structured AMn_{1-x}B_xO₃ (A = Ca or Ba; B = Fe or Ni) redox catalysts for partial oxidation of methane, *Catal. Sci. Technol.* 6 (2016) 4535–4544, <http://dx.doi.org/10.1039/C5CY02186C>.

[39] N. Galinsky, A. Mishra, J. Zhang, F. Li, Ca_{1-x}MnO₃ (A=Sr and Ba) perovskite based oxygen carriers for chemical looping with oxygen uncoupling (CLOU), *Appl. Energy*. 157 (2015) 358–367, <http://dx.doi.org/10.1016/j.apenergy.2015.04.020>.

[40] N. Galinsky, M. Sendi, L. Bowers, F. Li, CaMn_{1-x}B_xO_{3-δ}(B = Al, V, Fe, Co, and Ni) perovskite based oxygen carriers for chemical looping with oxygen uncoupling (CLOU), *Appl. Energy* 174 (2016) 80–87, <http://dx.doi.org/10.1016/j.apenergy.2016.04.046>.

[41] J.A. Sofranko, F. Li, L. Neal, Oxygen Transfer Agents for the Oxidative Dehydrogenation of Hydrocarbons and Systems and Processes Using the Same, WO2016049144, (2016) . (Accessed 5 March 2018) <https://patentscope.wipo.int/search/en/detail.jsf?docId=WO2016049144>.

[42] M. Rydén, H. Leion, T. Mattisson, A. Lyngfelt, Combined oxides as oxygen-carrier material for chemical-looping with oxygen uncoupling, *Appl. Energy*. 113 (2014) 1924–1932, <http://dx.doi.org/10.1016/j.apenergy.2013.06.016>.

[43] A. Shulman, E. Cleverstam, T. Mattisson, A. Lyngfelt, Manganese/Iron, Manganese/Silicon oxides used in Chemical-Looping with Oxygen Uncoupling (CLOU) for Combustion of Methane, *Energy Fuel* 23 (2009) 5269–5275, <http://dx.doi.org/10.1021/ef9005466>.

[44] A. Shulman, E. Cleverstam, T. Mattisson, A. Lyngfelt, Chemical – looping with oxygen uncoupling using Mn/Mg-based oxygen carriers – oxygen release and reactivity with methane, *Fuel* 90 (2011) 941–950, <http://dx.doi.org/10.1016/j.fuel.2010.11.044>.

[45] J.A. Sofranko, J.J. Leonard, C.A. Jones, A.M. Gaffney, H.P. Withers, Catalytic oxidative coupling of methane over sodium-promoted Mn/SiO₂ and Mn/MgO, *Catal. Today* 3 (1988) 127–135, [http://dx.doi.org/10.1016/0920-5861\(88\)87003-2](http://dx.doi.org/10.1016/0920-5861(88)87003-2).

[46] C.A. Jones, J.J. Leonard, J.A. Sofranko, Hydrocarbon Dehydrogenation, US4737595, (1988) (Accessed 1 March 2018), <https://patentimages.storage.googleapis.com/11/63/92/e0613c9ac03a/US4737595.pdf>.

[47] Y.T. Chua, A.R. Mohamed, S. Bhatia, Oxidative coupling of methane for the production of ethylene over sodium-tungsten-manganese-supported-silica catalyst (Na-W-Mn/SiO₂), *Appl. Catal. A Gen.* 343 (2008) 142–148, <http://dx.doi.org/10.1016/j.apcata.2008.03.032>.

[48] S. Ji, Surface WO₄ tetrahedron: the essence of the oxidative coupling of methane over M_WMn/SiO₂ catalysts, *J. Catal.* 220 (2003) 47–56, [http://dx.doi.org/10.1016/S0021-9517\(03\)00248-3](http://dx.doi.org/10.1016/S0021-9517(03)00248-3).

[49] A. Palermo, J.P. Holgado Vazquez, R.M. Lambert, New efficient catalysts for the oxidative coupling of methane, *Catal. Letters* 68 (2000) 191–196, <http://dx.doi.org/10.1023/A:1019072512423>.

[50] K. Okada, Y. Kameshima, A. Yasumori, Chemical shifts of silicon X-ray photoelectron spectra by polymerization structures of silicates, *J. Am. Ceram. Soc.* 81 (2005) 1970–1972, <http://dx.doi.org/10.1111/j.1151-2916.1998.tb02579.x>.

[51] A.P. Grosvenor, E.M. Bellhouse, A. Korinek, M. Bugnet, J.R. McDermid, XPS and EELS characterization of Mn₂SiO₄, MnSiO₃ and MnAl₂O₄, *Appl. Surf. Sci.* 379 (2016) 242–248, <http://dx.doi.org/10.1016/j.apsusc.2016.03.235>.

[52] M. Arjmand, M. Rydén, H. Leion, T. Mattisson, A. Lyngfelt, Sulfur tolerance and rate of oxygen release of combined Mn-Si oxygen carriers in chemical-looping with oxygen uncoupling (CLOU), *Ind. Eng. Chem. Res.* 53 (2014) 19488–19497, <http://dx.doi.org/10.1021/ie503687u>.

[53] B.A. Pinaud, Z. Chen, D.N. Abram, T.F. Jaramillo, Thin films of sodium birnessite-type MnO₂: optical properties, electronic band structure, and solar photoelectrochemistry, *J. Phys. Chem. C* 115 (2011) 11830–11838, <http://dx.doi.org/10.1021/jp200015p>.

[54] J.L. Junta, M.F. Hochella, Manganese (II) oxidation at mineral surfaces: a microscopic and spectroscopic study, *Geochim. Cosmochim. Acta* 58 (1994) 4985–4999, [http://dx.doi.org/10.1016/0016-7037\(94\)90226-7](http://dx.doi.org/10.1016/0016-7037(94)90226-7).

[55] H.W. Nesbitt, D. Banerjee, Interpretation of XPS Mn(2p) spectra of Mn oxyhydrates and constraints on the mechanism of MnO₂ precipitation, *Am. Mineral.* 83 (1998) 305–315, <http://dx.doi.org/10.2138/am-1998-3-414>.

[56] H. Mazurek, Molten Salt Hydrocarbon Conversion Process Using Oxygen Containing Feed, US4678862, (1987) (Accessed 1 March 2018), <https://patentimages.storage.googleapis.com/34/c1/c3/09913ab3116/US4678862.pdf>.